Oxidation of Metals, Vol. 47, Nos. 1/2, 1997

The Effect of Various Oxide Dispersions on the Phase Composition and Morphology of Al_2O_3 Scales Grown on β-NiAl

B. A. Pint,* M. Treska,† and L. W. Hobbs†

Received October 25, 1995; revised April 22, 1996

A series of oxide-dispersed β-NiAl alloys were oxidized in order to explore the effect of various cation dopants on the θ–α phase transformation in the Al_2O_3 scale and the effect of phase composition on the scale microstructure. Larger ions such as Y, Zr, La, and Hf appeared to slow the θ- to α-Al_2O_3 phase transformation, while a smaller ion, Ti, appeared to accelerate the transformation.

KEY WORDS: β-NiAl; oxide dispersion; reactive elements; θ-Al_2O_3, phase transformation.

INTRODUCTION

The formation of an external oxide or scale is essential for high-temperature oxidation resistance. In order to be protective, a scale must be dense, slow-growing, relatively chemically inert, and adherent. For high-temperature applications up to 1000°C, chromia-forming alloys, such as stainless steels, are widely used. However, at higher temperatures, the volatility of Cr_2O_3 limits its effectiveness as a protective scale. Because of the lower volatility and slower growth rate of Al_2O_3, alumina-forming alloys and coatings are more widely used at higher temperatures. Thus, as application temperatures increase, research efforts have increasingly focused on the nucleation and growth of alumina scales.

While earlier studies often assumed that the alumina scale formed during oxidation was α-Al_2O_3, numerous studies[1–20] have clearly identified the

*Metals and Ceramics Division, Oak Ridge National Laboratory, Oak Ridge, TN 37831-6156.
†H. H. Uhlig Corrosion Laboratory, Massachusetts Institute of Technology, Cambridge, MA 02139.

0030-770X/97/0200-0001$12.50/0

formation of metastable, cubic Al_2O_3 scales such as γ, δ, and θ. The formation of these metastable alumina phases at temperatures from 800 to 1200°C is significant for high-temperature oxidation because their subsequent transformation to α-Al_2O_3 can have a major effect on the oxidation behavior of an alloy. For instance, θ-Al_2O_3 scales are less dense and faster growing than α-Al_2O_3 scales.[10,12,15,18,19] The scales grow by different transport mechanisms[7,17,19,20] and have different microstructures. The metastable aluminas tend to form a bladelike morphology.[5,10–12,18–19]. Also of particular significance is the phase transformation from cubic to hexagonal trigonal, which results in a 13% volume reduction in the scale. Doychak and co-workers[3,5,6,8–11] studied the alumina scale microstructure on Zr-doped β-NiAl and developed a model in which the volume reduction, which occurs when the initially formed δ- or θ-Al_2O_3 scale transforms to α-Al_2O_3, leads to scale cracking. Transverse cracks through the scale thickness allow rapid oxidation and, ultimately, the formation of surface ridges in the scale. The ridge structure appears to be unique to aluminides, such as β-NiAl, and is not observed in the scales formed on MCrAl-type alloys.[13,14,21]. Several studies have indicated that the effect of the Al_2O_3 phase transformation is most acute for oxidation temperatures of 900–1100°C.[1,4,10,13–15,19] At higher temperatures, the initial alumina scales are typically α.

Phase transformations in Al_2O_3 are also important in the manufacture of catalysts, where the high surface area of γ-Al_2O_3 is a useful property. Unlike high-temperature oxidation, catalyst applications seek to retain the metastable phases for long periods of time; thus, research has been directed toward preventing the phase transformation in order to increase the lifetime and/or operating temperature of catalysts. Doping with a few percent of various oxides appears to inhibit the phase transformation.[22–24] A model by Burtin and co-workers[23] suggested that large ions enter the open, cubic lattice and there inhibit the transformation to the hexagonal α structure.

Recent work demonstrated that Zr or ion-implanted Y in β-NiAl slows the transformation of the θ-Al_2O_3 scale to α-Al_2O_3 in comparison to undoped β-NiAl.[16,18,19] Elements such as Y and Zr are common additions to high-temperature alloys because they improve α-Al_2O_3 scale adhesion.[25–27] The current work explores the effect of various oxide dispersions in β-NiAl on the scale phase composition and morphology. By using a range of dopant cation radii and studying the development of the scale microstructure, the models of Burtin and Doychak were tested for the formation of alumina scales on β-NiAl.

EXPERIMENTAL PROCEDURES

Gas-atomized β-NiAl (49 at.% Al) powder and 1 vol.% dopant oxide powder (Y_2O_3, La_2O_3, HfO_2, TiO_2, ZrO_2, Al_2O_3) were mechanically

Table I. Chemical Composition of the Oxide-Dispersed NiAl Alloys in Atomic Percent, Obtained by Inductively Coupled Plasma Analysis[29]

NiAl alloys	1 vol.% ZrO_2	1 vol.% Y_2O_3	1 vol.% La_2O_3	1 vol.% TiO_2	1 vol.% HfO_2	1 vol.% Al_2O_3
Ni	49.08	48.91	48.87	46.70	48.35	49.89
Al	48.29	48.13	46.94	44.99	47.67	47.31
Fe	0.03	0.02	0.03	0.14	0.11	0.15
Cr	0.03	0.03	0.03	0.06	0.04	0.05
Si	0.18	<0.01	0.12	n.d.	0.18	0.21
Ti	n.d.	<0.01	<0.01	0.33	n.d.	n.d.
Co	n.d.	n.d.	n.d.	0.02	n.d.	n.d.
Dopant	0.275 (Zr)	0.243 (Y)	0.235 (La)	0.334 (Ti)	0.298 (Hf)	—
Other	<0.01 (Y)	<0.01 (Zr)	<0.01 (Y)	0.001 (Y)	0.005 (Zr)	0.005 (Y)
Other			<0.01 (Zr)	0.004 (Mo)	<0.01 (Y)	<0.01 (Zr)
C	0.11	0.008	<0.01	0.24	0.25	<0.01
N	0.26	n.d.	0.11	0.12	0.10	0.28
O	1.76	2.66	3.67	7.40	3.24	2.11
S (ppm)	4	38	<3	<10	14	<3

blended in a nitrogen gas atmosphere using a water-cooled, high-speed attritor and steel balls. The attritor tank and balls were cleaned between runs in order to minimize cross-contamination. After blending, the powders were canned and degassed, and then extruded at 1232°C. The final chemical compositions are shown in Table I. This powder-metallurgy process produces a uniform microstructure, independent of oxide addition. Transmission electron microscopy of several compositions showed that the as-extruded grain size was approximately 1 μm. A large fraction of submicron Al_2O_3 particles was formed during the milling process, and the oxide particles were observed mainly at alloy grain boundaries.[28]

Oxidation coupons ($\approx$12 mm diameter $\times$ 1 mm thick) were polished to 0.3-μm alumina and ultrasonically cleaned in acetone and methanol prior to oxidation. Oxidation experiments were conducted at 1000°C and 1200°C in dry, flowing O_2. Specimens were rapidly inserted and removed from a hot furnace. Weight changes were measured continuously using a Cahn model 1000 microbalance. Samples were also weighed before and after oxidation using a Mettler model AE240 balance.

After oxidation, samples were examined using scanning electron microscopy with X-ray energy-dispersive spectroscopy (SEM/XEDS). A Rigaku X-ray powder diffractometer, with a 12-kW rotating anode source and equipped with a glancing angle (GAXRD) attachment, was used to analyze the thin alumina scales with a 0.5° incident angle.

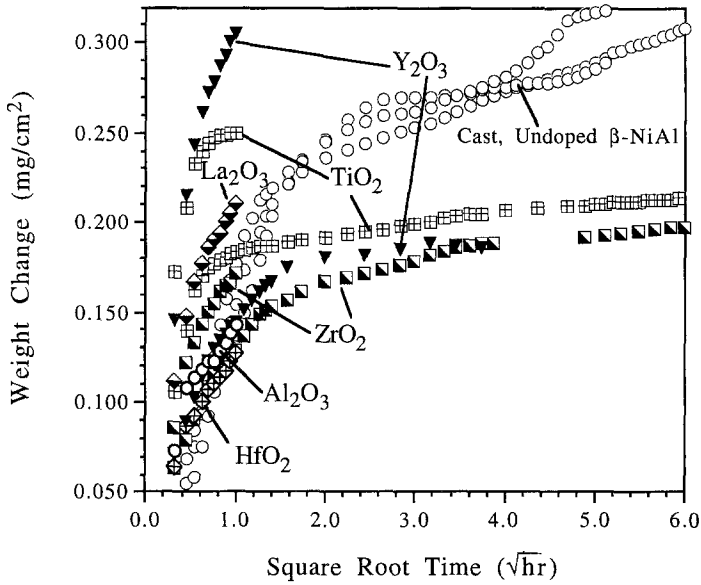

Fig. 1. Parabolic plot of weight gain versus square root of time for various β-NiAl alloys at 1000°C in 1 atm O_2. In general, the period of faster scale growth is reduced with the addition of an oxide dispersion compared to that observed on undoped, cast β-NiAl.

RESULTS

Oxidation studies commonly include kinetics weight-gain measurements in order to quantify the parabolic rate constant. In this study, kinetics were measured using thermal gravimetric analysis (TGA). A parabolic plot of weight gains at 1000°C is shown in Fig. 1. In general, the data follow the results found in other studies[10,15,16,18] where the initial oxidation rate is very high, but after $\approx$1 h the rate is sharply reduced. This change in rate was attributed by Rybicki and Smialek[10] to the change from metastable alumina formation to a slower-growing α-Al_2O_3 scale. Compared to undoped, cast β-NiAl,[18] the addition of an oxide dispersion appears to shorten the transition time to the slower growth rate. However, the kinetics in Fig. 1 do not clearly differentiate any effects of the various oxide dispersions. The scatter in the weight gains, particularly in the first few minutes of oxidation, appears to be greater than any dopant effect. An effort was made to standardize the data by setting the weight gain at 0.1 h to zero and by attempting to match the final weight gain measured at temperature by TGA to the weight gain measured after cooling (Table II). The first approach reduced the scatter significantly but still did not show much effect of the various additions; the

Table II. Measured Weight Gains (mg/cm^2) After Cooling to Room Temperature of Various β-NiAl Alloys at 1000°C

Addition	Oxidation time 1 h	50 h	100 h
Cast, undoped[14]	0.03[a]–0.19	0.10[a]–0.28	
1 vol.% TiO_2	0.04	0.12	0.13[a]
1 vol.% Y_2O_3	0.14	0.19	0.15[a]
1 vol.% ZrO_2	0.10	0.13	0.08[a]
1 vol.% La_2O_3	0.14	0.12	
1 vol.% Al_2O_3	0.09	0.13	
1 vol.% HfO_2	0.10	0.07[a]	
0.11 at.% Zr[14,18]	0.13	0.24	0.41
2×10^{16} Y/cm^2 implant[14,18]	0.13	0.23–0.37	0.45

[a] Measured weight gains may be lower due to scale spallation.

second did not produce reconcilable data sets, perhaps because the weight gains measured after cooling may be reduced by scale spallation. Unfortunately, the low weight gains, combined with problems in settling the balance in the early stages of oxidation, make such gravimetric measurements particularly difficult.

Despite the inconclusive kinetics data, significant differences in scale microstructures were observed using SEM. After 1-h oxidation at 1000°C, the most commonly observed microstructure was a mixture of fine-grain (submicron) blades and smoother patches (Fig. 2a). Previous TEM and GAXRD work[5,10–12,18–19] has linked the bladelike morphology to metastable aluminas such as θ-Al_2O_3. The smoother patches appeared to correspond to the location of oxide particles in the alloy. The dispersed oxides (both alumina and the dopant oxide) may thus affect the scale nucleation and growth. Fine cracks in the scale were observed in many of these smooth areas. The type of scale morphology was observed for additions of Zr, Y, and Hf. The addition of La also produced a similar microstructure, except that the blades appeared to be larger and more pronounced (Fig. 2b).

A very different microstructure was observed on the Al_2O_3-dispersed substrate (Fig. 2c). In this case, a very fine ridge-type structure was observed along with fine oxide nodules. Virtually no bladelike grains were observed. The addition of TiO_2 also produced a ridge-type morphology (Fig. 2d), although somewhat different from the structure on the alumina-dispersed β-NiAl. Unlike in the other scales, with Al_2O_3 and TiO_2 additions the morphologies appeared very uniform and did not appear to be locally affected by oxide particles in the alloy.

To further characterize the microstructure, GAXRD was used to determine the scale phase compositions. A peak-height comparison was used in

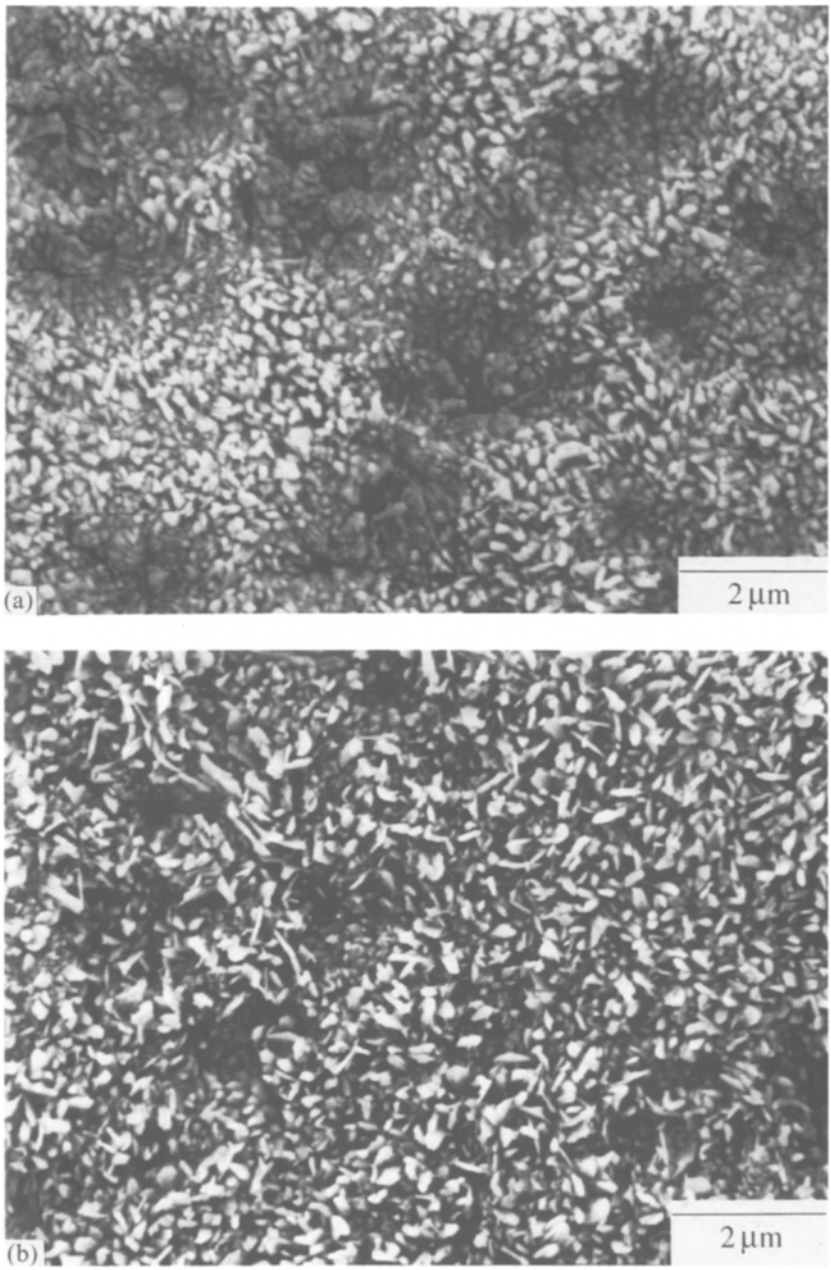

Fig. 2. SEM secondary-electron images of the alumina scale formed after oxidation for 1 h at 1000°C on β-NiAl with oxide dispersions of (a) HfO_2, (b) La_2O_3, (c) Al_2O_3, and (d) TiO_2.

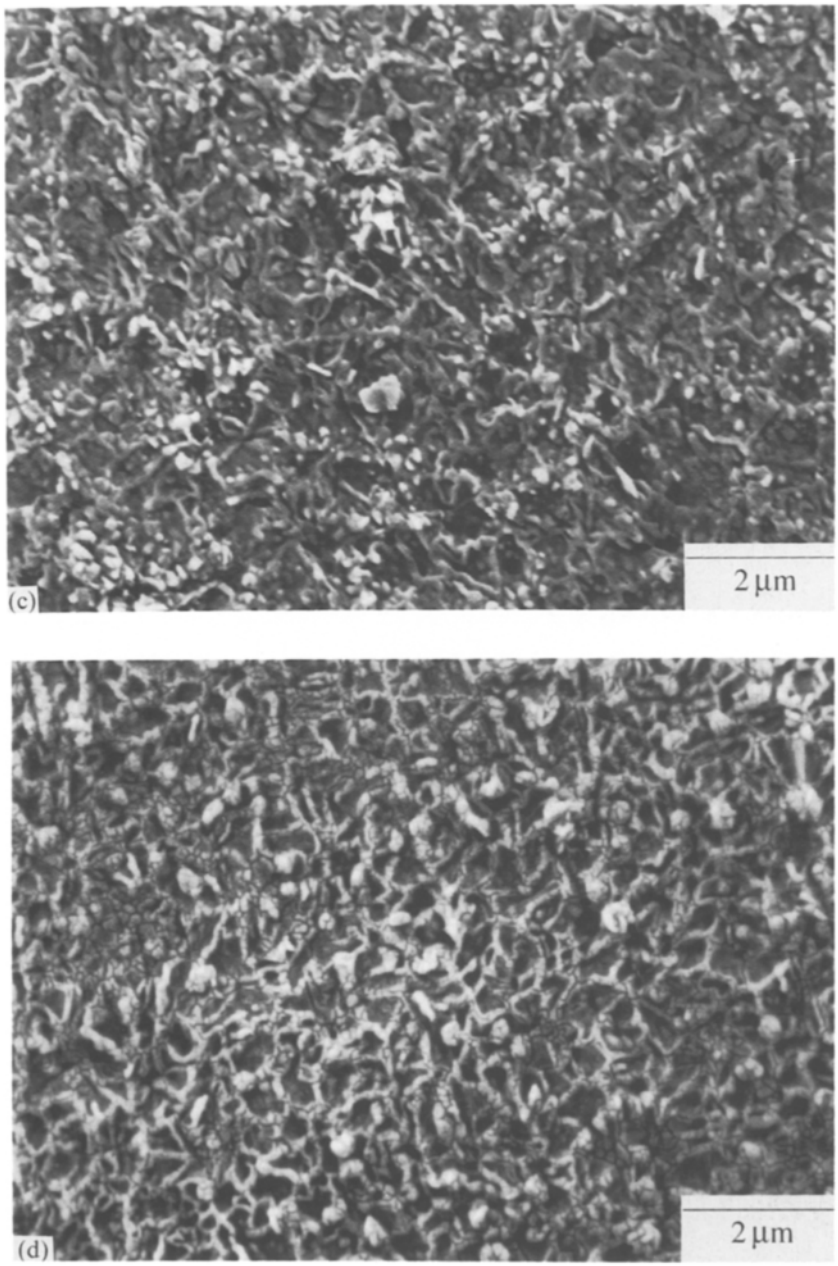

Fig. 2. Continued.

Table III. Phase Composition (%θ-Al_2O_3) of Scales Grown on Various β-NiAl Alloys at 1000°C After Several Exposures (0% indicates scale is 100% α-Al_2O_3)[a]

Alloy	Ni–50Al[18]	Ni–49Al	Ni–50Al[18]
Dopant	None	Y	Y
Method of addition	—	Oxide dispersion	2×10^{16} cm^{-2} ion implant
After 1 h	25%*	59%	99%
After 50 h	0%	0%	95%
After 100 h	0%	0%	86%

Alloy	Ni–49Al[18]	Ni–49Al	Ni–49Al
Dopant	Zr	Zr	Ti
Method of addition	0.11 at.% alloy addition	oxide dispersion	oxide dispersion
After 1 h	91%	60%	0%
After 50 h	0%	0%	0%
After 100 h	0%	0%	0%

Alloy	Ni–49Al	Ni–49Al	Ni–49Al
Dopant	Hf	La	Al
Method of addition	oxide dispersion	oxide dispersion	oxide dispersion
After 1 h	60%	51%	0%
After 50 h	0%	0%	0%
After 100 h	ND	ND	ND

[a] The oxide-dispersed alloys were extruded from powder and the other alloys were cast.
[b] Average of four samples, standad deviation of 30%.

order to make a semiquantitative approximation of the scale phase fractions.[13,16,18] Table III lists the percentage of θ-Al_2O_3 in the scales on several different alloys after various isothermal oxidation exposures. The percentage was obtained by using unobstructed peaks from θ-Al_2O_3 ($2\theta =$ 32.8° with Cu–Kα radiation) and α-Al_2O_3 (57.5°). Scales with bladelike morphologies after 1 hr (Figs. 2a and 2b) had 50–60% θ-Al_2O_3, while the ridge-type morphologies (Figs. 2c and 2d) were 100% α-Al_2O_3. Despite the larger blades on the La_2O_3-dispersed substrate (Fig. 2b), no corresponding increase in the fraction of θ-Al_2O_3 was detected. The amount of θ-Al_2O_3 present in the scale was less when the dopant was added as an oxide dispersion (ZrO_2 or Y_2O_3), compared with an elemental addition (0.11 at.% Zr)

or Y ion implantation.[16,18] Comparing undoped cast NiAl[16,18] with Al_2O_3-dispersed NiAl, the amount of θ-Al_2O_3 in the scale after 1-h oxidation was also reduced in the latter case. This is in agreement with the kinetics results (Fig. 1), where oxide additions generally reduced the transient, higher-rate time period.

Longer oxidation experiments also were conducted at 1000°C. After a 50-h exposure, none of the scales on the oxide-dispersed substrates had detectable θ-Al_2O_3 X-ray peaks (Table III). However, the scale morphologies were still significantly different, particularly those grown on TiO_2- and Al_2O_3-dispersed β-NiAl (Fig. 3). The ZrO_2-doped scale had only a few bladelike grains remaining after 50-h (Fig. 3a). Oxide ridges were beginning to develop, particularly in the smooth areas around oxide particles where cracks were observed after 1-h. A similar scale structure was observed on the La_2O_3-dispersed material.

The HfO_2-doped scale exhibited fewer oxide blades and more of a ridge-type structure (Fig. 3b). The Y_2O_3-doped scale showed fewer ridges but more pronounced oxide blades than on any of the other compositions (Fig. 3c). The scale on Al_2O_3-dispersed β-NiAl had a very pronounced, but close-packed, ridge structure (Fig. 3d). The ridge structure is typical of undoped α-Al_2O_3 scales, but generally the ridges are more widely spaced. Unlike the other materials, the fine ridges on the TiO_2-doped scale after 1-h had almost completely disappeared after 50 h (Fig. 3e). The remnant surface topography was by far the smoothest of any of the alloys in this study.

Several compositions were oxidized for 100 h at 1000°C. In general, the structures coarsened but did not change significantly. The scale microstructure on TiO_2-dispersed β-NiAl was virtually unchanged compared to that after 50 h. The ridges on the ZrO_2-doped scale continued to grow and became more pronounced. In contrast, the Y_2O_3-doped scale exhibited less ridge formation, and the oxide blades were less pronounced after 100 h than after 50 h. The blades appear not to be growing but to be slowly transforming to α. Interestingly, at lower magnifications the remnants of the oxide blades appeared to form a coarse network (Fig. 4), similar to the finer ridge network observed on the ZrO_2-doped scale.

A more obvious differentiation of the effects of the different dispersoids was observed in the early stages of oxidation at 1200°C. At 1200°C, there was very little indication of any θ-Al_2O_3 formation. The additions of ZrO_2, HfO_2, and La_2O_3 produced a ridge-type morphology, similar to the α-Al_2O_3 scales formed on other cast NiAl materials[8,10,18,20,29,30] (Fig. 5a). The ridges were closer-packed on HfO_2-dispersed β-NiAl but similar in appearance. The ridges were less pronounced on the Y_2O_3-doped scale (Fig. 5b).

Similar to results at 1000°C, the Al_2O_3 and TiO_2-dispersed materials oxidized at 1200°C produced far different scale morphologies. The scale on Al_2O_3-dispersed β-NiAl had a very fine ridge structure, with a ridge at

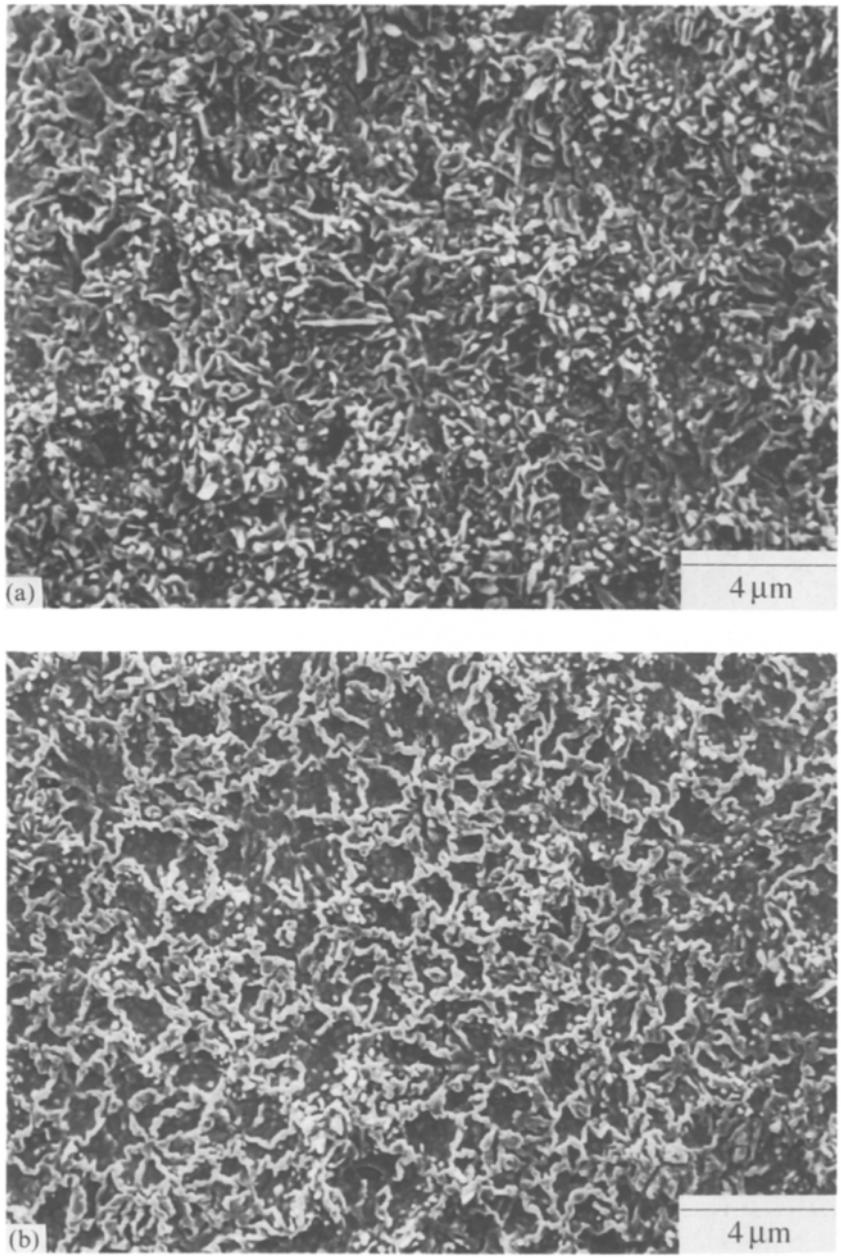

Fig. 3. SEM secondary-electron images of the alumina scale formed after oxidation for 50 h at 1000°C on β-NiAl with oxide dispersions of (a) ZrO_2, (b) HfO_2, (c) Y_2O_3, (d) Al_2O_3, and (e) TiO_2.

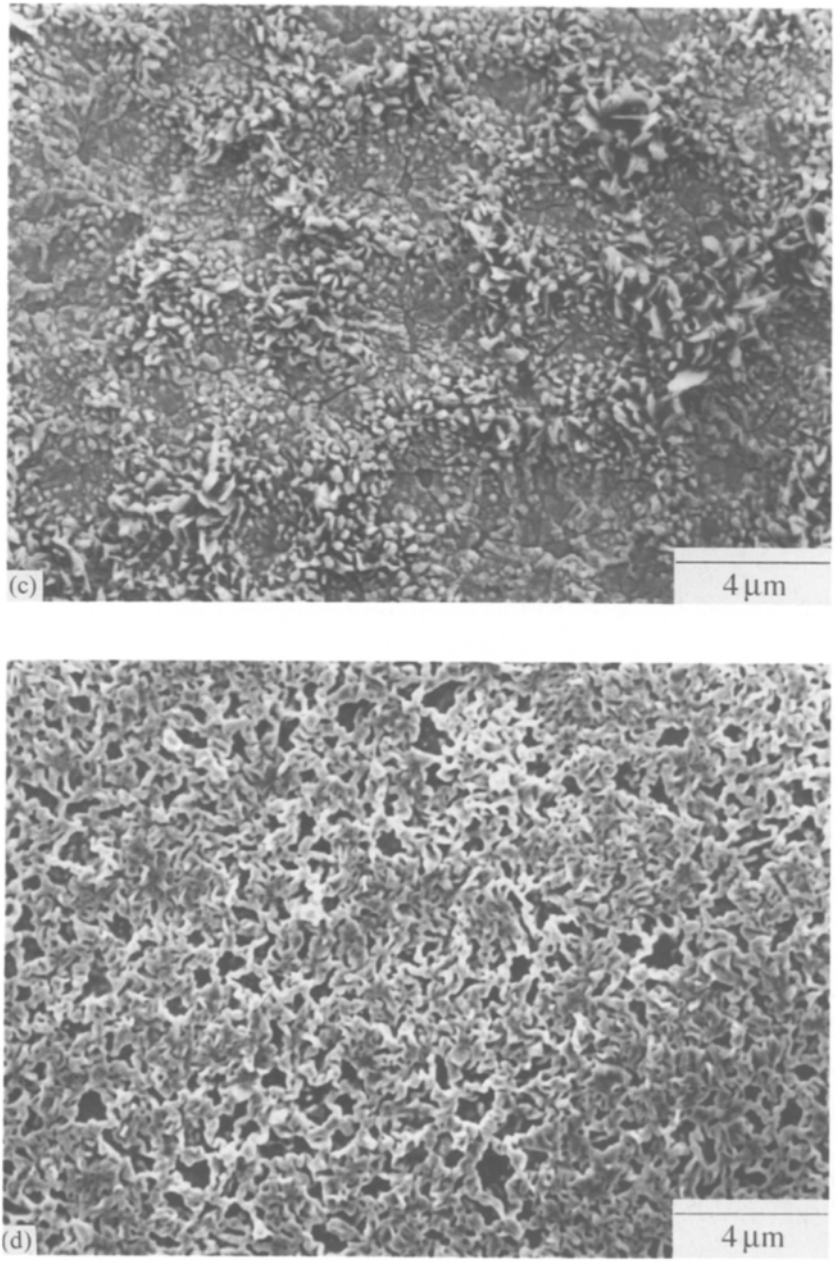

Fig. 3. Continued.

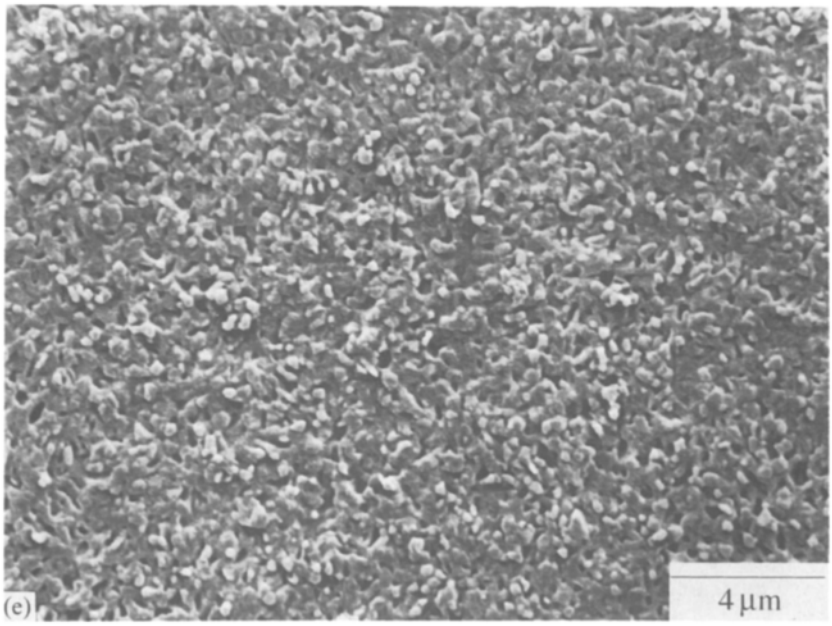

Fig. 3. Continued.

nearly every scale grain boundary (Fig. 5c). The TiO_2-doped scale showed no evidence of any type of ridge structure (Fig. 5d). Individual grains were clearly delineated, and fine microcracks were observed on the surface. This structure is very similar to that observed on a commercial Y_2O_3-dispersed Fe–20 at.% Cr–10% Al–0.39% Ti (Inco Alloy MA956) oxidized under the same conditions.[21,31]

DISCUSSION

Although not obvious from the weight gain kinetics, alumina scale composition and morphology are strongly influenced by different oxide dispersants in β-NiAl. Clearly, there was some effect from the presence of an oxide dispersion in general, but there was also a separate chemical-doping effect on the scale. In general, these observations appear to corroborate the models proposed by Burtin[23] and Doychak.[6,8]

For oxidation at 1000°C, variations in scale morphology are not reflected in significant differences in the kinetics data or in the weight gains. In general, the changes in scale morphology did not profoundly affect the oxidation behavior of the materials under the conditions used in this study.

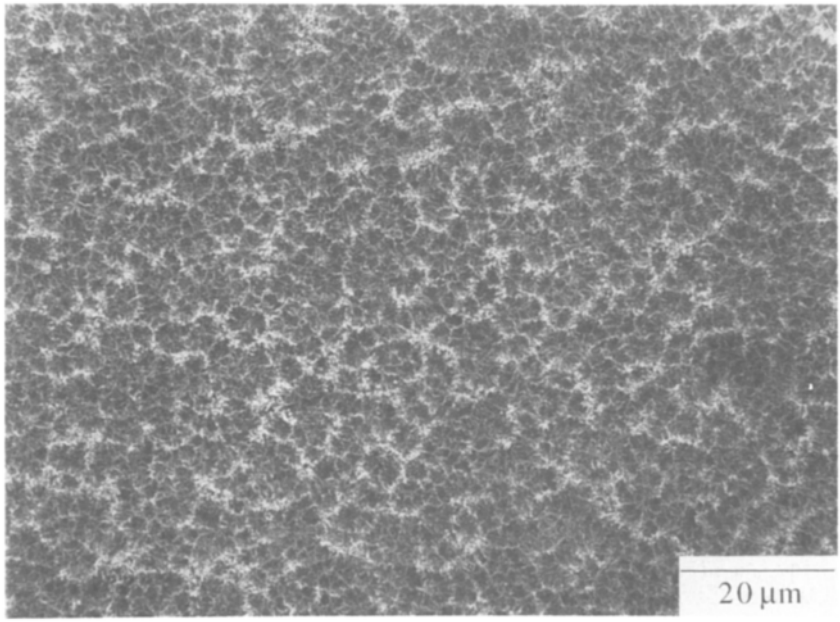

Fig. 4. SEM secondary-electron image of the alumina scale formed after oxidation for 100 h at 1000°C on β-NiAl with an oxide dispersion of Y_2O_3.

At higher temperatures ($\geq$1200°C), the various dopants did begin to have a more critical influence on the oxide scale growth rate and adhesion.[29] However, it is important to understand how these later-stage morphologies develop.

The initial fine grain size of the alloy ($\approx$1 μm) appears to mask any effect of crystallographic orientation on the scale morphology.[6,11,14,32,33] The oxide particles (both alumina and dopant oxide) probably also affect the initial nucleation of the scale.[34] In most cases, an oxide dispersion in the alloy appears to help nucleate α-Al_2O_3, resulting in a faster transformation from θ-Al_2O_3, than in cast β-NiAl with other types of additions (Table III). For example, the Al_2O_3-dispersed β-NiAl quickly formed an α-Al_2O_3 scale without the transient presence of θ-Al_2O_3 observed on cast, undoped β-NiAl. Also, the θ-Al_2O_3 percentages were lower with the addition of Y_2O_3 and ZrO_2 compared to implanted Y and alloyed Zr, respectively. The high oxygen contents found in these alloys (Table I) indicates a large fraction of Al_2O_3 particles relative to the dopant oxide particles. However, no clear correlation can be drawn between alloy oxygen content and scale phase composition or morphology. Thus, a simple nucleation effect does not appear to explain all of the observations, and it is necessary to look at chemical effects to explain the influence or the various dopants. For example,

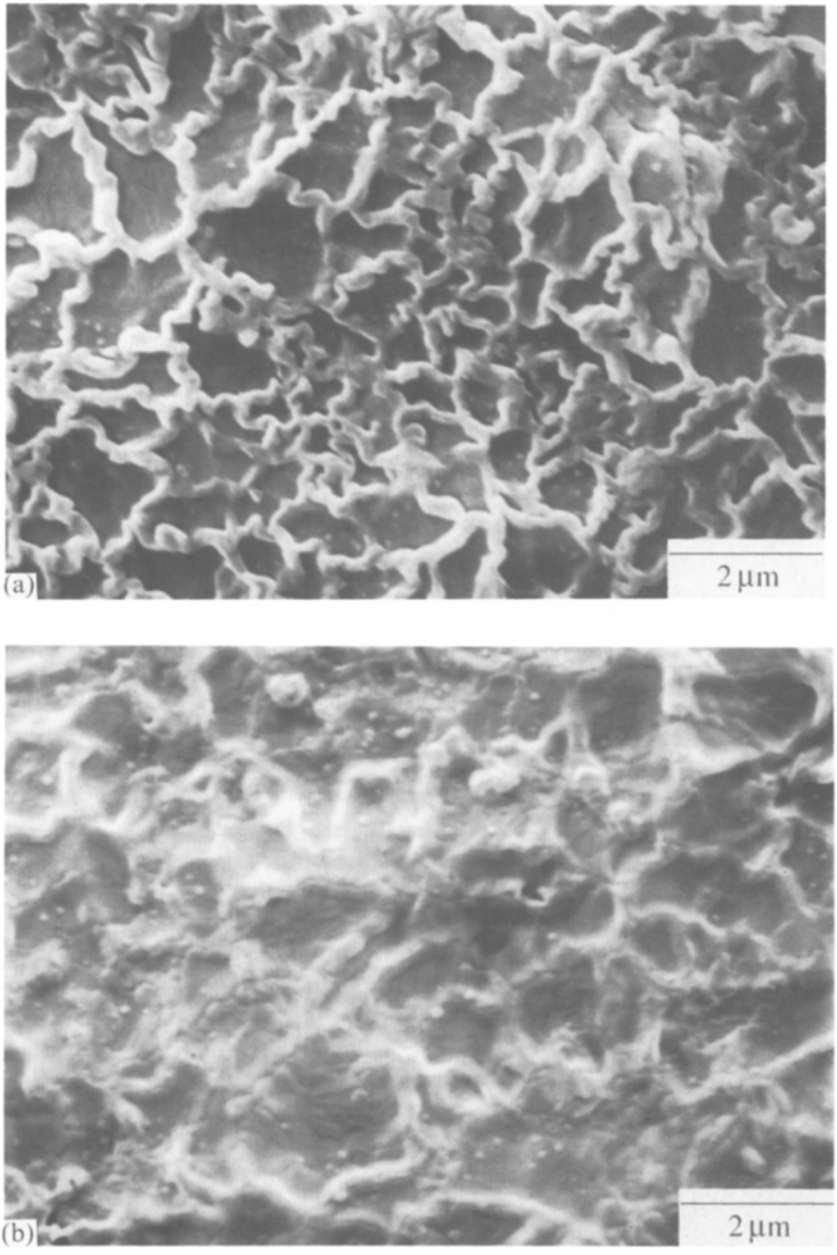

Fig. 5. SEM secondary-electron images of the alumina scale formed after oxidation for 2 h at 1200°C on β-NiAl with oxide dispersions of (a) La_2O_3, (b) Y_2O_3, (c) Al_2O_3, and (d) TiO_2.

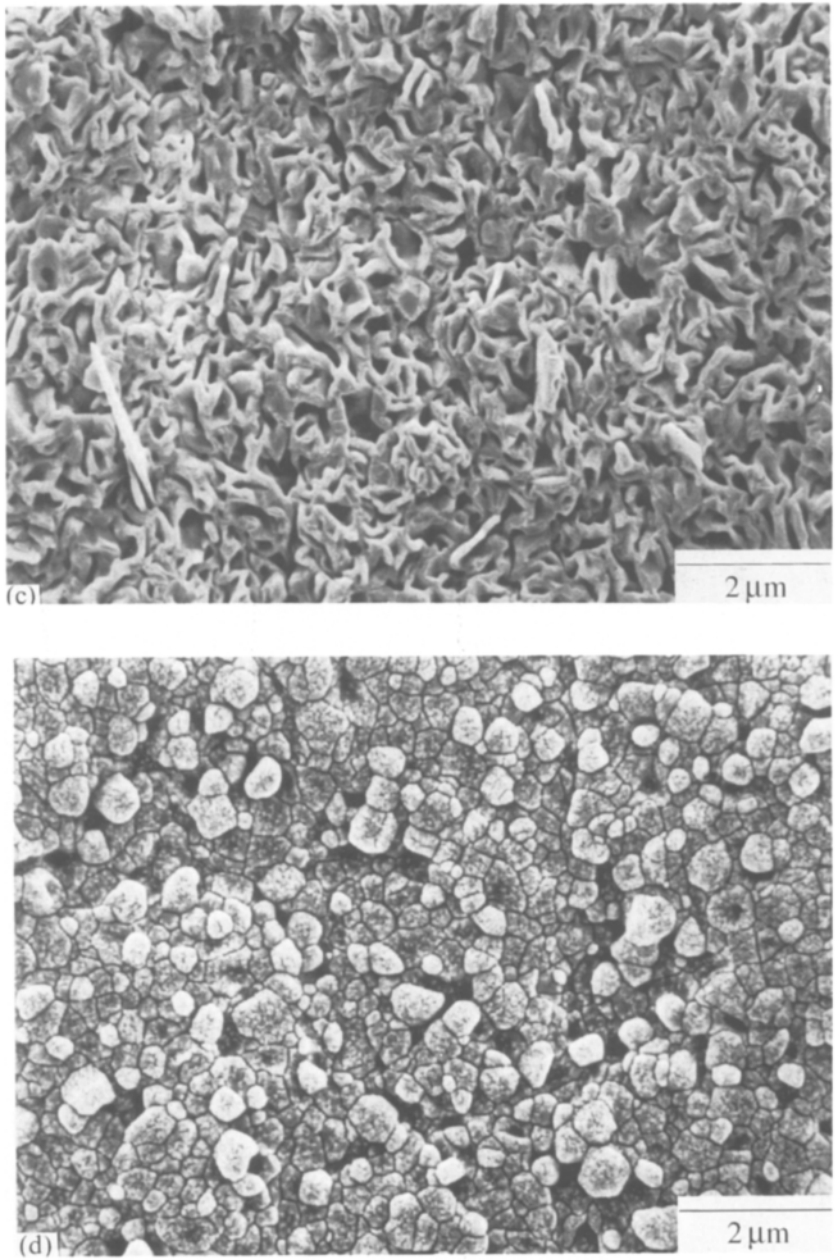

Fig. 5. Continued.

Table IV. Ionic Radii of Various Cations Using Coordination Number of 6

Cation	Ionic radii
Al^{3+}	0.53
Hf^{4+}	0.71
La^{3+}	1.06
Ti^{4+}	0.61
Y^{3+}	0.89
Zr^{4+}	0.72

the more pronounced oxide blades on the La_2O_3-dispersed alloy (Fig. 2) or the reduction in ridge growth on the Y_2O_3-doped scale (Figs. 3 and 5) must reflect chemical effects.

The model proposed by Burtin *et al.*[23] emphasizing ion size and dopant valence appears to account for a number of the present observations. Burtin observed that larger ions, such as Ca, La, and Th, tend to inhibit the θ–α phase transformation, while smaller ions, such as Mg and Ga, accelerate the transformation to α. Valence plays a role in intermediate-size ions, with higher valence ions (such as Zr) acting as inhibitors.

The Burtin model would appear to explain the observation that a TiO_2 addition did not inhibit the scale transformation to α-Al_2O_3, relative to the behavior of undoped cast β-NiAl (Table III). The Ti ion is similar in size to Mg and Ga, which Burtin found to be accelerators.[23] The larger ions added in this study (Table IV) all appear to have acted as inhibitors. While there appear to be some differences in scale morphologies among the large-ion additions (Hf, La, Y, and Zr), each had a similar effect on the scale phase composition (Table III). Based on their larger ionic size and the longer-term presence of bladelike oxide grains (typical of θ-Al_2O_3[5,10–12,18–19]), Y and La appear to be the most effective inhibitors. This conclusion is also consistent with the Burtin model, since La and Y are larger ions than Zr or Hf. However, it is difficult to draw firm conclusions about the relative effectiveness of the various additions, because the oxide additions were added as identical volume fractions (1%) rather than as equal atomic percent additions, which would better identify the effectiveness of the various dopants.

The exact mechanism whereby larger ion dopants inhibit the θ- to-α phase transformation has not been demonstrated explicitly. Burtin suggested that reducing the surface area (sintering) of the metastable alumina is a critical step in the transformation and that the rate-limiting step is vacancy annihilation. It has also been suggested that large ions in the relatively open cubic lattice inhibit the diffusionless, martensitic- or shear-type transformation from cubic to hexagonal Al_2O_3.[35] Thus, the dopant could play a role

at the surface or within the lattice. Since sintering would seem to be more of a concern with Al_2O_3 powders, a dopant effect on the Al_2O_3 lattice would seem more plausible in the case of growing scales. A large dopant ion, such as La or Y, could distort the surrounding cubic Al_2O_3 lattice, thus stalling a diffusionless transformation from θ to α by requiring more energy to overcome the distortion.

The oxide-morphology model proposed by Doychak *et al.*[6,8] also appears to explain many of the observations for these materials. However, in describing Al_2O_3 morphologies, it is important to distinguish two types of ridges: the "extrinsic" type which (as described by Doychak) form as a result of the θ–α Al_2O_3 phase transformation (e.g., Figs 3b and 5a); and finer, "intrinsic" ridges which are observed on undoped α-Al_2O_3[21] (e.g., Fig. 5c). It is proposed that extrinsic ridges form when the scale cracks as a result of the volume reduction associated with the phase transformation and at regions where growing α-Al_2O_3 nuclei intersect. These ridges form during the initial transient stage of oxidation but do not grow significantly (relative to scale thickness) during steady-state oxidation.[14] Intrinsic ridges are thought to form on each oxide grain boundary and grow by the outward transport of Al through the scale, during steady-state oxidation. Intrinsic ridges do not form on α-Al_2O_3 scales which are doped with a reactive element such as Y or Zr, presumably because these elements suppress short-circuit Al transport.[17,21,36]

In agreement with the Doychak model, the typical formation of extrinsic oxide ridges at the gas interface is observed when the transient θ-Al_2O_3 phase develops initially. Particularly with the larger ion dopants (Hf, La, Y, and Zr), the progression of blades (e.g. Figs. 2a, b) to cracks (e.g., Fig. 3c) to ridges (Figs. 3a, b) seems to be followed. The scale morphology on Y_2O_3-dispersed β-NiAl after 100 h at 1000°C would indicate that some coarser ridges may form from the remnants of the last remaining θ-Al_2O_3 blades when they transform to the α phase. However, the same basic ridge-type morphology is found on this material as well.

With the Al_2O_3- and TiO_2-dispersed materials, this same progression appears to occur more rapidly and the resulting morphology is far different. The very fine ridges observed after 1 h at 1000°C (Figs. 2c, d) appear to be extrinsic ridges, thus indicating that a phase transformation occurred in the very early stages of exposure at 1000°C. It is unlikely that these are outward growing, intrinsic ridges, because they do not correspond to scale grain boundaries on either material. With an earlier transformation to α-Al_2O_3, ridges on both materials formed on a finer scale than on the other alloys where the transformation to α was inhibited. At longer times, this resulted in a closer-packed ridge structure (Figs. 3d, e). In the case of the TiO_2 dispersion, little trace of the ridge structure was observed after 50 or 100 hr.

The clearly defined intrinsic ridges on the Al_2O_3-dispersed β-NiAl observed at 1200°C and the more pronounced extrinsic ridges after 50 hr at 1000°C (Fig. 3d) both may be a result of the outward transport of Al through the scale. In each of the other materials, the dopant ions could inhibit Al diffusion by segregating to the α-Al_2O_3 scale grain boundaries.[17,21,37] In a study of these and other materials, each of these dopant ions (Hf, La, Ti, Y, and Zr) has been found to segregate to grain boundaries in α-Al_2O_3 scales grown at 1200°C.[38]

A question remains regarding whether TiO_2 can be considered an accelerator. Because of the high oxygen content (meaning a higher fraction of Al_2O_3 particles in the alloy than the other materials), it is difficult to separate the effect of the Ti dopant from the oxygen content. Rather than Ti accelerating the transformation, the larger fraction of oxide particles may have nucleated α more quickly. However, based on observations of TiO_2 dispersions in FeCrAl and β-NiAl alloys and small Ti alloy additions to β-NiAl,[39] it appears that the presence of Ti does have a substantial effect on the morphology of α-Al_2O_3, including an effect on the θ–α phase transformation.

CONCLUSIONS

A series of oxide-dispersed β-NiAl alloys were oxidized in order to explore the effect of various cation dopants on the θ–α phase transformation in the Al_2O_3 scale, and the effect of the phase composition on the scale microstructure. The oxide-dispersed alloys formed scales with higher α-Al_2O_3 fractions than cast alloys with dopants added by other techniques. Differences were observed among the various dopant oxide dispersions. Larger ions such as Y, Zr, La, and Hf appeared to slow the θ- to α-Al_2O_3 phase transformation, while a smaller ion, Ti, appeared to accelerate the transformation. Slowing the phase transformation enhances the formation of a ridge-type morphology. "Extrinsic" ridges form as a result of scale cracking during the phase transformation. However, when the phase transformation is not inhibited, the scale morphology is very different and the ridge-type morphology is obscured. These results support the models proposed by Burtin and co-workers on the Al_2O_3 phase transformation and Doychak and co-workers on the formation of oxide-scale ridges.

ACKNOWLEDGMENTS

The authors are grateful to Homogeneous Metals, Clayville, New York, for the NiAl powder, Dr. R. Mason and Prof. N. Grant at MIT for assistance with the powder blending, and Dr. J. D. Whittenberger and Dr. J. Doychak at NASA Lewis for extruding the OD NiAl alloy and providing the cast

NiAl ingots. This work was begun at MIT with support from the Electric Power Research Institute. BAP is currently funded by the U.S. Department of Energy Distinguished Postdoctoral Research Program administered by the Oak Ridge Institute for Science and Education. The research at ORNL was sponsored by the Division of Materials Sciences, U.S. Department of Energy, under contract De-AC05-96OR22464 with Lockheed Martin Energy Research Corp. The most current work at MIT was supported by the National Science Foundation under grant #DMR-9022640.

REFERENCES

1. W. Hagel, *Corrosion* **21**, 316 (1965).
2. T.A. Ramanarayanan, M. Raghavan, and R. Petkovic-Luton *Trans. Jpn. Inst. Met.* **24**, 199 (1983).
3. J. Doychak, in *Proceedings of the 42nd Annual Meeting of the Electron Microscopy Society of America*, G. W. Bailey, ed. (San Francisco Press, San Francisco, CA, 1984), pp. 598–599.
4. P. T. Moseley, K. R. Hyde, B. A. Bellamy, and G. Tappin, *Corros. Sci.* **24**, 547 (1984).
5. J. K. Doychak, T. E. Mitchell, and J. L. Smialek, in *High Temperature Ordered Intermetallic Alloys I*, MRS Symp. Proc. vol. 39, Boston, MA, 1984, C. C. Koch, C. T. Liu, and N. S. Stoloff, eds. (MRS, Pittsburgh, PA, 1985), pp. 475–484.
6. J. Doychak, Ph.D. thesis (Case Western Reserve University, Cleveland, OH, 1986).
7. P. A. van Manen, E. W. A. Young, D. Schalkoord, C. J. van der Wekken, and J. H. W. de Wit, *Surf. Interface Anal.* **12**, 391 (1987).
8. J. Doychak, J. L. Smialek, and C. A. Barrett, in *Oxidation of High-Temperature Intermetallics*, T. Grobstein and J. Doychak, eds. (TMS, Warrendale, PA, 1988), pp. 41–55.
9. J. Doychak and M. Ruhle, *Oxid. Met.* **31**, 431 (1989).
10. G. C. Rybicki and J. L. Smialek, *Oxid. Met.* **31**, 275 (1989).
11. J. Doychak, J. L. Smialek, and T. E. Mitchell, *Metall. Trans.* **20A**, 499 (1989).
12. B. A. Pint, A. Jain, and L. W. Hobbs, in *High Temperature Ordered Intermetallics IV*, Symp. Proc. vol. 213, L. A. Johnson, D. P. Pope, and J. O. Steigler, eds. (MRS, Pittsburgh, PA, 1991), pp. 981–986.
13. W. J. Quadakkers, K. Schmidt, H. Grubmeier, and E. Wallura, *Mater. High Temp.* **10**, 23 (1992).
14. B. A. Pint, Ph.D. thesis (Massachusetts Institute of Technology, Cambridge, MA, 1992).
15. M. W. Brumm and H. J. Grabke, *Corros. Sci.* **33**, 1677 (1992).
16. B. A. Pint, A. Jain, and L. W. Hobbs, in *High Temperature Ordered Intermetallics V*, Symp. Proc. vol. 288, I. Baker, R. Darolia, J. D. Whittenberger, and M. H. Yoo, eds. (MRS, Pittsburgh, PA. 1993), pp. 1013–1018.
17. B. A. Pint, J. R. Martin, and L. W. Hobbs *Oxid. Met.* **39**, 167 (1993).
18. B. A. Pint and L. W. Hobbs, *J. Electrochem. Soc.* **141**, 2443 (1994).
19. B. A. Pint, J. R. Martin, and L. W. Hobbs, *Solid State Ionics* **78**, 99 (1995).
20. M. J. Graham, D. F. Mitchell, R. Prescott, and J. Doychak, *Electrochemical Society Extended Abstracts* **94–2**, 837 (1994); manuscript submitted to *Corros. Sci.*
21. B. A. Pint, A. J. Garratt-Reed, and L. W. Hobbs, submitted to *Mater. High Temperature.*
22. H. Schaper, E. B. M. Doesburg, and L. L. Van Reijen, *Appl. Catal.* **7**, 211 (1983).
23. P. Burtin, J. P. Brunelle, M. Pijolat, and M. Soustelle, *Appl. Catal.* **34**, 225 (1987).
24. M. Ozawa, M. Kimura, and A. Isogai, *Mater. Sci. Lett.* **9**, 709 (1990).
25. E. Lang (ed.) *The Role of Active Elements in the Oxidation Behavior of High Temperature Metals and Alloys* (Elsevier Applied Science, London, 1989).
26. W. E. King (ed.) *The Reactive Element Effect on High Temperature Oxidation—After Fifty Years*, Materials Science Forum **43** (Trans Tech Publications, Switzerland, 1989).

27. R. Prescott and M. J. Graham, *Oxid. Met.* **38**, 233 (1992).
28. B. A. Pint and K. B. Alexander, manuscript in progress.
29. B. A. Pint, submitted.
30. R. Prescott, D. F. Mitchell, G. I. Sproule, and M. J. Graham, *Solid State Ionics* **53–56**, 229 (1992).
31. B. A. Pint, *Electrochemical Society Extended Abstracts* **94–2**, 835–836 (1994).
32. T. Homma, H. Hindam, Y. Pyun, and W. W. Smeltzer, *Oxid. Met.* **17**, 223 (1982).
33. J. P. Roux, M. W. Brumm, and H. J. Grabke, *Fresenius J. Anal. Chem.* **346**, 265 (1993).
34. J. Stringer, B. A. Wilcox, and R. I. Jaffee, *Oxid. Met.* **5**, 11 (1972).
35. J. R. Wynnyckyj and C. G. Morris, *Metall. Trans.* **16B**, 345 (1985).
36. W. J. Quadakkers, H. Holzbrecher, K. G. Briefs, and H. Beske, *Oxid. Met.* **32**, 67 (1989).
37. B. A. Pint, *Oxid. Met.* in press.
38. B. A. Pint, A. J. Garratt-Reed, and L. W. Hobbs, submitted.
39. B. A. Pint, unpublished research.